Low-frequency Noise Characterization of Si Nanonet Field Effect Transistors

Thibauld Cazimajou
IMEP-LaHC
Univ Grenoble Alpes,
Univ. Savoie Mont Blanc,
CNRS, Grenoble INP
Grenoble, France
thibauld.cazimajou@grenoble-inp.fr

Christoforos Theodorou
IMEP-LaHC
Univ Grenoble Alpes,
Univ. Savoie Mont Blanc,
CNRS, Grenoble INP
Grenoble, France
christoforos.theodorou@grenoble-inp.fr

Maxime Legallais
IMEP-LaHC, LMGP, LTM
Univ Grenoble Alpes,
Univ. Savoie Mont Blanc,
CNRS, Grenoble INP
Grenoble, France
maxime.legallais@cea.fr

Thi Thu Thuy Nguyen
LMGP
Univ Grenoble Alpes,
Univ. Savoie Mont Blanc,
CNRS, Grenoble INP
Grenoble, France
thuthuynguyen2004@gmail.com

Mireille Mouis
IMEP-LaHC
Univ Grenoble Alpes,
Univ. Savoie Mont Blanc,
CNRS, Grenoble INP
Grenoble, France
mouis@minatec.grenoble-inp.fr

Celine Ternon
LMGP, LTM
Univ Grenoble Alpes,
CNRS, Grenoble INP
Grenoble, France
celine.ternon@grenoble-inp.fr

Bassem Salem
LTM
Univ Grenoble Alpes,
CNRS, CEA
Grenoble, France
bassem.salem@cea.fr

Gerard Ghibaudo
IMEP-LaHC
Univ Grenoble Alpes,
Univ. Savoie Mont Blanc,
CNRS, Grenoble INP
Grenoble, France
gerard.ghibaudo@grenoble-inp.fr

***Abstract*— This paper deals with the low frequency noise characterization of silicon nanonet field effect transistors. Electrical noise parameters such as surface trap density and remote Coulomb scattering coefficient were extracted using the carrier number and correlated mobility fluctuation model. Their variation with density of nanowires and source-drain distance is presented, as well as a method to obtain information about the order of magnitude of the electrical active area variation.**

Random network; silicon nanowire; electronic transport; Low frequency noise; percolation

I. Introduction

Nanowire (NW) based field effect transistors (FET) seem to be promising building blocks for biosensing applications, because of the NW sensitivity to surface charge [1]. However, their large scale integration can be complex. In the Front-End-of-Line, it normally requires processes for nanowires patterning, as well as a touchy etching process through the thick Back-End-of-Line stack, in order to open an access to the active nanowire-based channel. Moreover, a minimum opening size is required to allow fluid penetration, thus increasing footprint and cost [2]. Other integration concepts could be adapted from the techniques that have been developed for CNT-based transistors [3], allowing for above-IC integration. However, being based on essentially aligned nanostructures, these techniques would be limited to the fabrication of short devices, with a source-drain distance smaller than the mean nanostructure length. Here instead, the active material is a network of randomly interconnected nanowires, also called nanonet (NN). Silicon Nanonets can be fabricated using low-cost bottom-up processes, they can be transferred on any type of substrate and they can be processed using standard microelectronics technology [4]. The thermal budget required for such processing is compatible with CMOS integration (maximum temperature below 400°C) [5]. This opens the route to the 3D integration of sensor arrays above their CMOS readout. The first NN-based FET has been obtained recently [5] and has been studied through static measurements [6]. In this paper, we present an analysis of the low frequency noise (LFN) measurements performed for different densities of NWs and source-drain distance L_{mask}. Furthermore, we demonstrate a method to extract the apparent density of oxide interface traps. Finally, based on its dependence with NW density and source-drain distance, we present a model approach for the physical active area variation.

II. Devices under study

The NNs used in this study were self-assembled from Si-NWs grown by Vapor Liquid Solid chemical vapor deposition [6]. NW length and diameter were respectively 7 µm ± 3 µm and 40 nm ± 7 nm. NNs can be fabricated with different NW densities [8]. For this paper, 4 different densities (from d = 0.28 NWs.µm^{-2} to 0.66 NWs.µm^{-2}) NNs were then transferred on a Si / Si_3N_4 wafer passivated with alumina and contacted by Ni / Au metal pads. Field-effect control was obtained by using the Si / (200nm) Si_3N_4 substrate as a backgate. Several device geometries were available with Source-Drain (S-D) distance L_{mask} ranging from 5 µm to 1000 µm and a constant pad width W_{mask} = 200 µm. For this study, only devices with L_{mask} = 30 µm and 50 µm were tested. In this case, because L_{mask} is longer than the average NW length, it means that the channel is made of several conduction paths where each path is constituted by a successive alternation of NWs and NW-NW junctions.

III. Experimental protocol and raw results

The drain current noise power spectral density (PSD) was measured in the low frequency range (4 Hz-10 kHz) in a metal

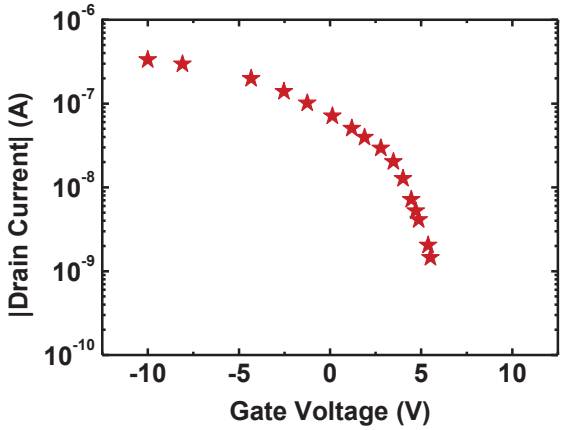

Fig. 1. Transfer characteristics I_d-V_g for the sample A (L_{mask} = 30µm et d = 0.28 NWs.µm^{-2})

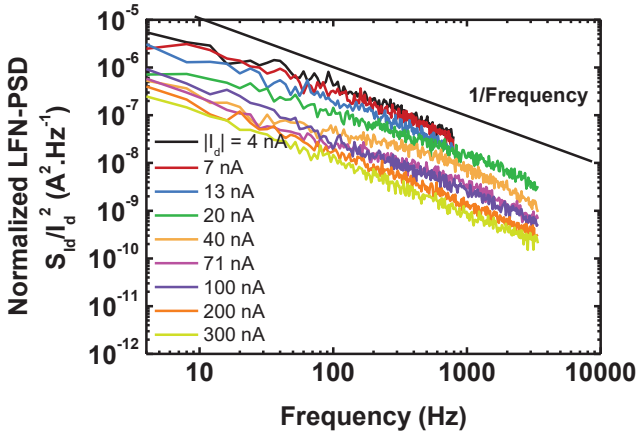

Fig. 2. LFN-PSD analysis for the sample A (d = 0.28 NWs.µm^{-2}, L_{mask} = 30 µm), for different I_d at V_d = -9V. Black line indicates 1/f dependency.

shielding box, as a function of back gate voltage (V_g), at room temperature. Source contact was grounded and drain contact was set at a given bias voltage (V_d = -9 V). A Programmable Point-Probe Noise Measurement System was employed. Fig. 1 shows typical I_d-V_g characteristic for sample A (with a NW density, d = 0.28 NWs.µm^{-2} and L_{mask} = 30 µm). Fig. 2 shows normalized drain current noise power spectral density (LFN-PSD) S_{id}/I_d^2 for sample A, for different values of drain current. The LFN-PSD is generally 1/f like, except for some Lorentzian contributions. The total LFN behavior can be attributed to a large ensemble of Lorentzian noise sources based on individual NWs and junctions between NWs.

IV. ANALYSIS AND DISCUSSION

Within the carrier number and correlated mobility fluctuation model (CNF-CMF), the drain current noise is given by:

$$\frac{S_{id}}{I_d^2} = \left(1 + \Omega \left(\frac{I_d}{g_m}\right)\right)^2 \left(\frac{g_m^2}{I_d^2}\right) S_{vfb} \qquad (1)$$

with flat band voltage PSD S_{vfb} and CMF factor $\Omega = \alpha\mu_{eff}C_{ox}$ [9] and α the remote Coulomb scattering coefficient. The flat band voltage PSD S_{vfb} is related to the oxide trap density N_{st} with the equation:

$$S_{vfb} = \frac{q^2 kTN_{st}}{WLC_{ox}^2 f} \qquad (2)$$

with electron charge q, Boltzmann constant k, temperature T, channel width W, channel length L, oxide capacitance C_{ox}, frequency f. In this case, the input referred gate voltage noise S_{Vg} now reads:

$$S_{vg} = \frac{S_{id}}{g_m^2} = \left(1 + \Omega \left(\frac{I_d}{g_m}\right)\right)^2 S_{vfb} \qquad (3)$$

Fig. 3 shows S_{vg} measured at f = 10 Hz as a function of drain current for sample A. A plateau is visible for small value of I_d, corresponding to S_{vg} equal to S_{vfb} (approximately equal to 2.10^{-6} V^2.Hz^{-1} for f = 10 Hz). The increase of S_{vg} in higher values of I_d can be attributed to the CMF component in (3) or to the access resistance. For sample A, S_{vfb}=2.10^{-6} V^2.Hz^{-1} for f = 10 Hz, and considering L_{mask} as L and W_{mask} as W, an apparent trap density can be extracted of about 10^{15} cm^{-2}.eV^{-1}.

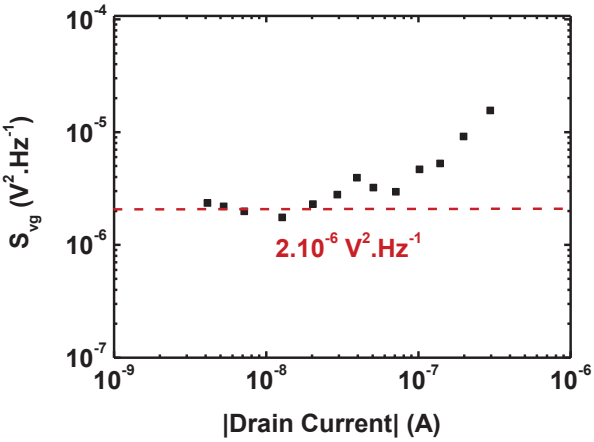

Fig.3. S_{vg} extracted at f=10Hz as a function of drain current for sample A. A plateau is visible at low current, corresponding to a S_{vfb} = 2.10^{-6} V^2.Hz^{-1}, and a trap density equal to 10^{15} cm^{-2}.eV^{-1}.

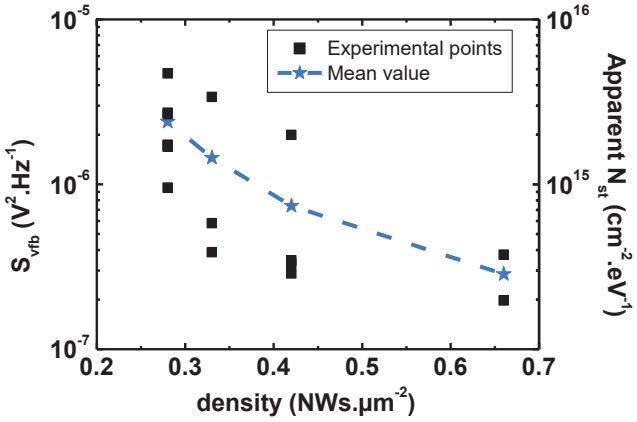

Fig.4. S_{vfb} extracted from plateau of S_{vg} and corresponding apparent trap density as a function of the density. Squares are for experimental points and stars for mean values. Dotted line is a guidance for the eyes.

Fig. 4 shows the extracted values of S_{vfb} from the weak inversion plateau of S_{vg}, and the corresponding apparent trap density, as a function of NW density for devices with L_{mask} = 30 µm. The apparent trap density decreases when the NW density increases. However, even though a dispersion of trap density value is expected from one device to another, a mean variation with the density is not reasonable. This apparent variation can be attributed to a variation of the electrical active area, especially of the physical width. Since $1/S_{vfb}$ reads,

$$\frac{1}{S_{vfb}} = \frac{fWLC_{ox}^2}{q^2kTN_{st}} \quad (4)$$

considering the typical description of conductance in percolating problem [10] and the small variation of channel length when the NW density increases (the average length of shortest conduction paths are found only 10% longer than L_{mask} in [9]), the channel width $W_{channel}$ can be described by the equation:

$$W_{channel} = cst \times (d - d_c)^{\beta} \quad (5)$$

with d_c the percolation threshold and β an exponent equal to 4/3 for 2D networks. In this case, considering (4) with $W_{channel}$ as W, $1/S_{vfb}$ should vary as:

$$\frac{1}{S_{vfb}} = cst' \times (d - d_c)^{\beta} \quad (6)$$

Fig. 5 shows the successful fit of the inverse of mean S_{vfb} with the model (6). Assuming $W_{channel}$ as W in (2), another trap density can be extracted. Fig. 6 shows this trap density as a function of the NW density. This N_{st} seems to be constant with the NW density increase. Because of the unknown value of the constant term in (5), the study of the mean value of N_{st} is meaningless. However, the difference between the apparent trap density value (approximately 5.10^{15} $cm^{-2}eV^{-1}$) extracted from LFN data and the trap density extracted from the subthreshold slope of the I-V data (7.10^{12} $cm^{-2}.eV^{-1}$) can provide an insight regarding the difference between the physical area ($W_{mask}L_{mask}$) and the effective (channel) area. The ratio between the two areas seems to be around 2 orders of magnitude.

Fig. 7 shows fits with CNF-CMF model of the normalized LFN-PSD of sample A as a function of I_d. One of the fits is realized without remote Coulomb scattering factor. These 2 fits show the importance of the remote Coulomb scattering in these devices ($\Omega = 0.14V^{-1}$). Extracted S_{vfb} ($S_{vfb} = 1.6.10^{-6}$ $V^2.Hz^{-1}$) is consistent with the one extracted by considering only the plateau of S_{vg}. Fig 8 shows $\alpha\mu_{eff}$ ($= \Omega/C_{ox}$) as a function of NW density for L_{mask} = 30 µm and L_{mask} = 50 µm. The mean value of $\alpha\mu_{eff}$ is in the order of 5.10^6 $cm^2.C^{-1}$ for L_{mask} = 30 µm. This value is consistent with the ones observed in silicon [11].

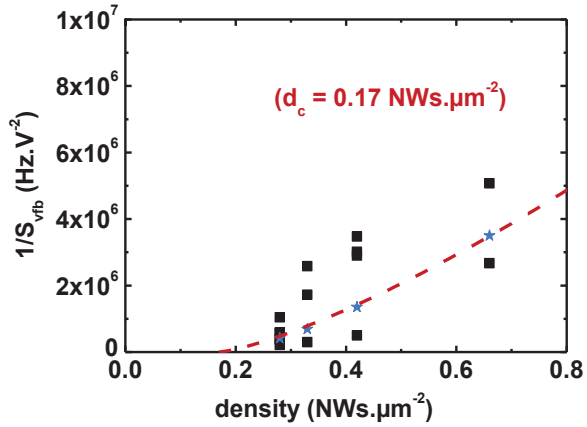

Fig.5. $1/S_{vfb}$ as a function of density. Square are for experimental points and stars for mean values. Red dotted line is the successful fit with the equation (6)

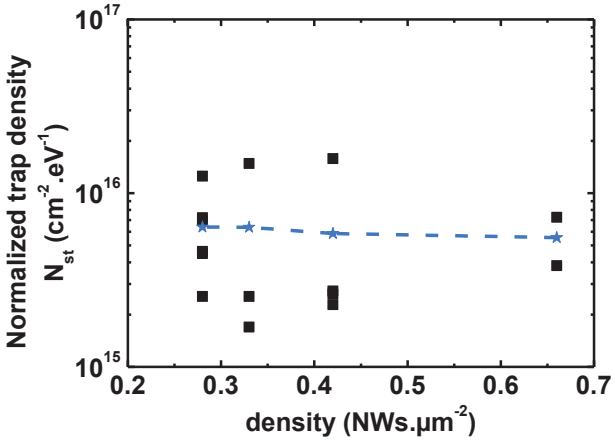

Fig.6. Trap density extracted from (3) with $W_{channel}$ as W as a function of the NW density. Squares are for experimental points and stars for mean values.

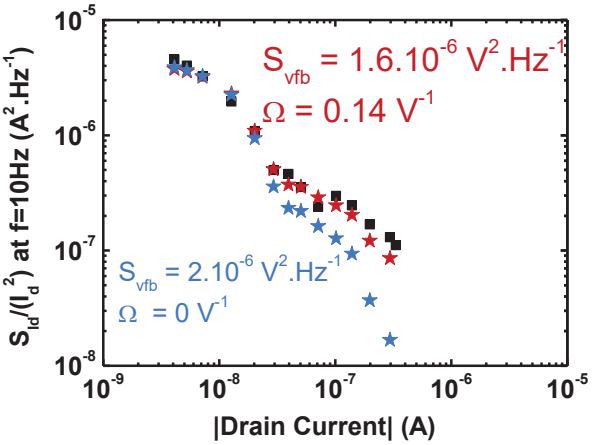

Fig.7. I_d normalized LFN-PSD at f = 10Hz (symbols) with CNF-CMF (stars) fitting curves for sample A. Blue stars correspond to a fit without remote coulomb scattering, and red stars correspond to a fit with remote Coulomb scattering.

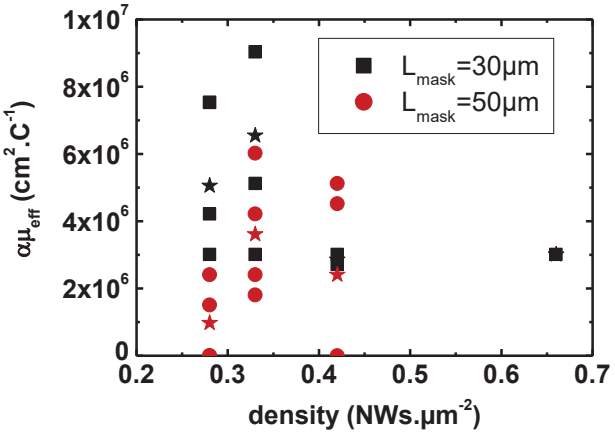

Fig.8. $\alpha\mu_{eff}$ as a function of NW density for different Source-drain distances. For L_{mask} = 30µm, black squares are experimental points and black stars mean values. For L_{mask} = 50µm, red circles are experimental points and red stars mean values.

For a small number of devices (Fig. 9), (1) does not fit the normalized LFN-PSD, because of an increase of S_{id}/I_d^2 in strong inversion regime. This increase can be related to the access resistance noise, which can be added to the model as:

$$\frac{S_{id}}{I_d^2} = (1 + \Omega\,(\frac{I_d}{g_m}))^2\,(\frac{g_m^2}{I_d^2})\,S_{vfb} + S_{Rsd}(g_d + \frac{g_m}{2})^2 \quad (7)$$

with S_{Rsd} the PSD of the access resistance [12]. With this equation, a good fit of S_{id}/I_d^2 is obtained, as shown in Fig. 9. Note that in general, the variation is that of Fig. 7 which cannot be well fitted with the assumption of a serial resistance noise but where account for CMF model is required.

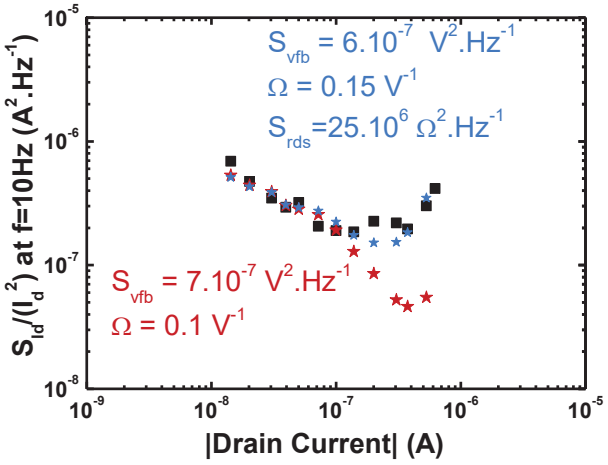

Fig.9. I_d normalized LFN-PSD at f = 10Hz (symbols) with CNF-CMF (stars) fitting curves, for a device with d = 0.28 NWs.µm^{-2} and L_{mask} = 30 µm. Red stars correspond to a fit with remote Coulomb scattering but without access resistance. Blue stars correspond to a fit with remote Coulomb scattering and access resistance.

V. Conclusion

We measured the LFN characteristics of passivated nanonet-based FET devices with different source-drain distances and NW densities. Flat band voltage PSD and remote Coulomb scattering factors were extracted using the CNF-CMF model. Apparent density of traps is extracted using S_{vfb} and the gate area. Comparison of this trap density with the one extracted from static measurement provides the ratio between the gate area and the real electrical active area where percolating transport occurs.

Acknowledgment

This work has received funding from the EU H2020 RIA project Nanonets2Sense under grant agreement n°688329. This work was partly supported by the French RENATECH network. This work benefited from the facilities and expertise of the OPE)N(RA characterization platform of FMNT (FR 2542, fmnt.fr) supported by CNRS, Grenoble INP and UGA.

References

[1] Y. Cui, Q. Wai, H. Park and C. M. Lieber, "Nanowire Nanosensors for Highly sensitive and selective detection of biological and chemical species", Sciences, vol.293, pp.1289-1292 (2001)

[2] G. Jayakumar, M. Legallais, P.-E. Hellström, M. Mouis, I. Pignot-Paintrand, V. Stambouli, et al., "Wafer-scale HfO2 encapsulated silicon nanowire field effect transistor for efficient label-free DNA hybridization detection in dry environment", Nanotechnology, vol. 30, Number 18 (2019)

[3] N. Patil, A. Lin, E. R. Myers, H.-S. P. Wong, and S. Mitra, "Integrated Wafer-Scale Growth and Transfer of Directional Carbon Nanotubes and Misaligned-Carbon-Nanotube-Immune Logic Structures", Symposium on VLSI Technology Digest of Technical Papers 2008

[4] G. Gruner, "Carbon nanonets spark new electronics", Sci. Am., vol.296 (5), pp.76–83, (2007)

[5] C. Ternon, P. Serre, J. M. Lebrun, V. Brouzet, M. Legallais, et al., "Low Temperature Processing to Form Oxidation Insensitive Electrical Contact at Silicon Nanowire/Nanowire Junctions," Adv. Electron. Mater., vol.1, Issue 10, 1500172 (2015)

[6] M. Legallais, T.T.T. Nguyen, M. Mouis, B. Salem, E. Robin, P. Chenevier, C. Ternon, "An innovative large scale integration of silicon nanowire-based field effect transistors", Solid-State Electronics 143, 97-107 (2018)

[7] T. Cazimajou, M. Legallais, M. Mouis, C. Ternon, B. Salem, G. Ghibaudo, "Electrical characteristics of silicon percolating nanonet-based Field Effect Transistors in the presence of dispersion", Solid-State Electronics 143, 83-89 (2018)

[8] P. Serre, C. Ternon, V. Stambouli, P. Periwal, T. Baron, "Fabrication of silicon nanowire networks for biological sensing", Sensors and Actuators B: Chemical 182, 390-395 (2013)

[9] M.-K. Joo, M. Mouis, D.-Y. Jeon, G.-T. Kim, U. J. Kim, and G. Ghibaudo, "Static and low frequency noise characterization of N-type random network of carbon nanotubes thin film transistors", Journal of Applied Physics, 114, 154503 (2013)

[10] D. Stauffer, and A.Aharony, "Introduction to Percolation Theory" (1994)

[11] M. Koyama, M. Cassé, R. Coquand, S. Barraud, G. Ghibaudo, H. Iwai, and G. Reimbold, "Study of Low - frequency Noise in SOI Tri - gate Silicon Nanowire MOSFETs", ICNF (2013)

[12] G.Ghibaudo and T.Boutchacha, "Electrical noise and RTS fluctuations in advanced CMOS devices", Microelectronics Reliability, 42, 573–582 (2002)